

# Supplementary online material for “A Multivariate Dynamic Statistical Model for the Global Carbon Budget 1959 – 2020”\*

*Mikkel Bennedsen<sup>(a)</sup> Eric Hillebrand<sup>(b)</sup> Siem Jan Koopman<sup>(c)</sup>*

<sup>(a)</sup>Department of Economics and Business Economics, Aarhus University, Denmark

<sup>(b)</sup>Corresponding author, Department of Economics and Business Economics, Aarhus University, Denmark

<sup>(c)</sup>Department of Econometrics, Vrije Universiteit Amsterdam, The Netherlands

December 20, 2022

## S1 Estimating nonlinear sink functions with time - varying coefficient models

We consider a number of different data-generating processes for this exercise, actual sink functions motivated by the application, but also linear and sine wave functions for generality. The simulation design is as follows. For all cases, the estimated model is a time-varying regression coefficient model that is estimated on the synthetically generated data.

$$\begin{aligned} S_t &= a + \beta_t C_t + \varepsilon_t, \quad \varepsilon_t \stackrel{i.i.d.}{\sim} \mathcal{N}(0, \sigma_\varepsilon^2), \\ \beta_{t+1} &= \beta_t + \eta_t, \quad \eta_t \stackrel{i.i.d.}{\sim} \mathcal{N}(0, \sigma_\eta^2). \end{aligned} \tag{1}$$

The first equation is the measurement equation that connects the unobserved component  $\beta_t$  to the synthetic sink data  $S_t$  by way of a time-varying and exogenously determined regressor value  $C_t$ . The second equation is the state equation that describes the time-varying regression coefficient process  $\beta_t$  as a random walk. The intention of this simulation exercise is to show that these random walk

---

\* Addresses: Mikkel Bennedsen, Department of Economics and Business Economics, Aarhus University, Fuglesangsallé 4, 8210 Aarhus V, Denmark, [mbennedsen@econ.au.dk](mailto:mbennedsen@econ.au.dk); Eric Hillebrand, Department of Economics and Business Economics, Aarhus University, Fuglesangsallé 4, 8210 Aarhus V, Denmark, [ehillebrand@creates.au.dk](mailto:ehillebrand@creates.au.dk); Siem Jan Koopman, Department of Econometrics, Vrije Universiteit Amsterdam, De Boelelaan 1105, 1081 HV Amsterdam, The Netherlands, [s.j.koopman@vu.nl](mailto:s.j.koopman@vu.nl)

dynamics are sufficiently flexible to capture, in-sample, a wide range of functions, including highly nonlinear ones. The objective is, therefore, not realism, neither in the values of the data-generating parameters nor in the range of values employed for atmospheric concentrations. It is, rather, to obtain a wide variety of functions to be fitted on a sample of the size considered in this paper.

**Linear.** In the linear case, we consider the data-generating process

$$S_t = -12.25 + 13.73 \frac{C_t}{C_0} + e_t,$$

where  $t = 1, \dots, 61$ ,  $\frac{C_t}{C_0} \in [1, 1.4]$  in 61 equidistant steps,  $e_t \stackrel{i.i.d.}{\sim} \mathcal{N}(0, 0.33)$ , and  $C_0 = 593\text{GtC}$ .

**Bacastow-Keeling.** We employ the sink function proposed by Bacastow and Keeling (1973) as the deterministic core and contaminate with a Gaussian error:

$$S_t = 1.5 + 2.5 \log \left( \frac{C_t}{C_0} \right) + e_t,$$

where  $t = 1, \dots, 61$ ,  $\frac{C_t}{C_0} \in [1, 7.4]$  in 61 equidistant steps,  $e_t \stackrel{i.i.d.}{\sim} \mathcal{N}(0, 0.33)$ .

**Gifford.** We employ the sink function proposed by Gifford (1993) as the deterministic core and contaminate with a Gaussian error:

$$S_t = \frac{0.005(C_t - C_b)}{1 + 0.0005(C_t - C_b)} + e_t,$$

where  $C_t$  is expressed in ppm, and thus  $C_t \in [279, 7.4(279)]$  in 61 equidistant steps,  $C_b = 31$  (atmospheric concentration at which net primary production vanishes),  $t = 1, \dots, 61$ ,  $e_t \stackrel{i.i.d.}{\sim} \mathcal{N}(0, 0.33)$ .

**Joos et al.** We employ the sink function proposed by Joos et al. (1996) as the deterministic core and contaminate with a Gaussian error:

$$\begin{aligned} S_t &= k \left[ C_t - \left( pCO2_0 + \sum_{j=1}^5 \frac{\delta_j C^j}{h^j A^j} \sum_{|\alpha|=j} \binom{j}{\alpha} (Sr)^\alpha \right) e^{\gamma(T_t - T_0)} \right] + e_t, \\ &= kC_t - kf(S_{t-1}, S_{t-2}, \dots, S_1) + e_t, \end{aligned}$$

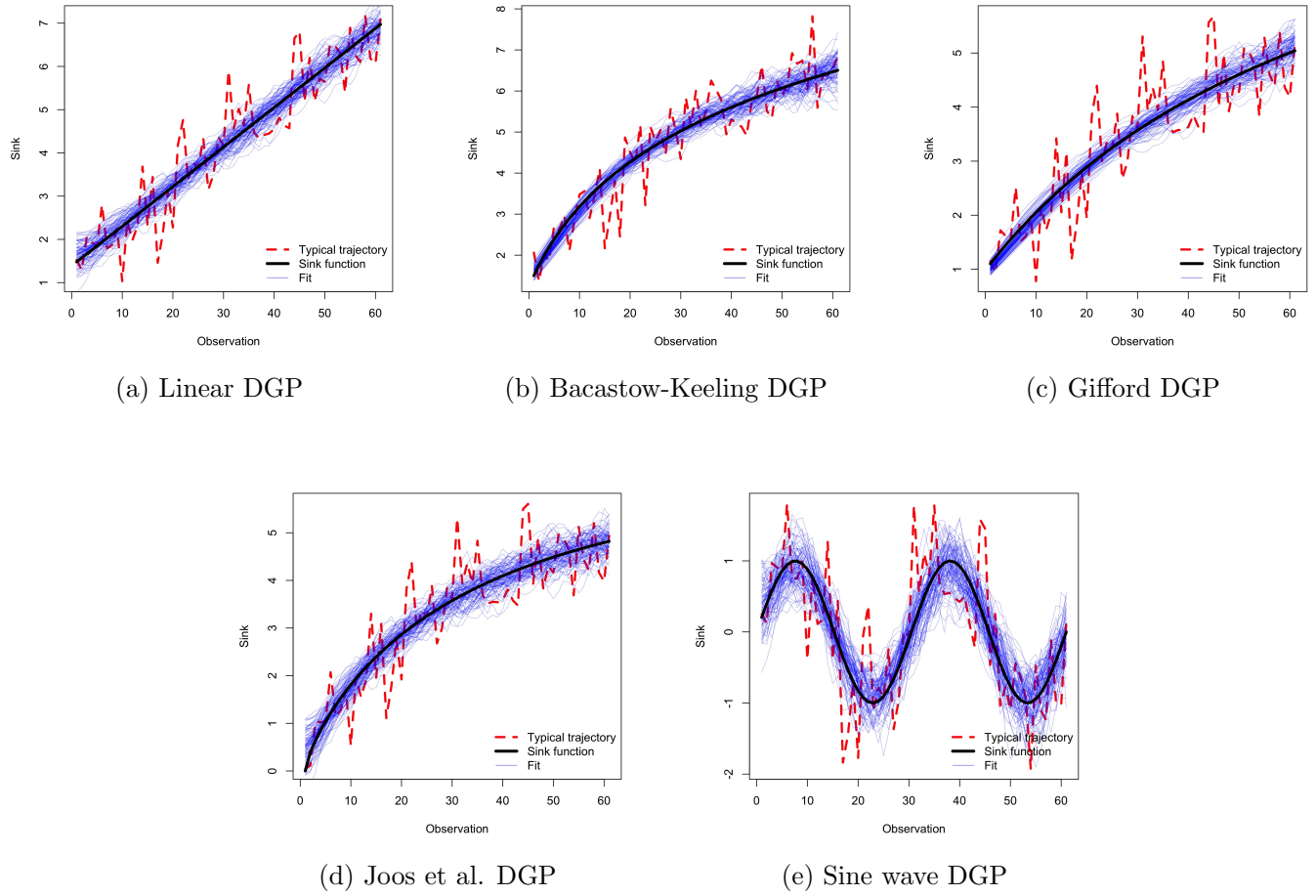
where  $C_t$  is expressed in ppm, and thus  $C_t \in [279, 7.4(279)]$  in 61 equidistant steps,  $t = 1, \dots, 61$ ,  $e_t \stackrel{i.i.d.}{\sim} \mathcal{N}(0, 0.33)$ , and

$$\begin{aligned}
k &= 0.10, \\
pCO2_0 &= 279 \text{ ppm}, \\
\delta_1 &= 1.5568 - 1.3993T_0 * 10^{-2}, \\
\delta_2 &= (7.4706 - 0.20207T_0) * 10^{-3}, \\
\delta_3 &= -(1.2748 - 0.12015T_0) * 10^{-5}, \\
\delta_4 &= (2.4491 - 0.126397T_0) * 10^{-7}, \\
\delta_5 &= -(1.5468 - 0.15326T_0) * 10^{-10}, \\
T_0 &= 18.2 \text{ C}, \\
c &= 1.722 * 10^{17} / 2.127 \mu\text{mol m}^3 / (\text{GtC} * \text{kg}), \\
h &= 75 \text{ m mixed layer depth}, \\
A &= 3.62 * 10^{14} \text{ m}^2 \text{ ocean area}, \\
\alpha &= (\alpha_1, \alpha_2, \dots, \alpha_{t-1}), \\
\binom{j}{\alpha} &= \frac{j!}{\alpha_1! \alpha_2! \cdots \alpha_{t-1}!}, \\
(Sr)^\alpha &= (S_1 r(t-1))^{\alpha_1} (S_2 r(t-2))^{\alpha_2} \cdots (S_{t-1} r(1))^{\alpha_{t-1}}, \\
r(t) &= \sum_{i=1}^6 \gamma_i e^{-\tau_i t}, \\
(\gamma_1, \tau_1) &= (0.014819, 0), \\
(\gamma_2, \tau_2) &= (0.70367, 1/0.70177), \\
(\gamma_3, \tau_3) &= (0.24966, 1/2.3488), \\
(\gamma_4, \tau_4) &= (0.066485, 1/15.281), \\
(\gamma_5, \tau_5) &= (0.038344, 1/65.359), \\
(\gamma_6, \tau_6) &= (0.019439, 1/347.55), \\
\gamma &= 0, \\
T_t &= \text{Surface temperature}.
\end{aligned}$$

Obviously this is a function whose time-series dynamic properties, in particular stability, are difficult to understand. But it is intuitively clear that given the rapidly declining weights in  $\delta_i$ , and given the

declining impulse response weights in  $r(t)$ , there are small enough values of  $k$  such that the feedback through the  $kf(S_{t-1}, S_{t-2}, \dots, S_1)$  term does not grow too large, and the  $kC_t$  term is dominant. Then, the sink process will be approximately linear in concentrations. We find that for values of  $k < 0.02$ , the function behaves approximately linearly on 61 observations, for  $k > 0.02$ , there is discernible curvature, and for  $k > 0.32$ , the feedback effects introduce oscillating explosive behavior. Since we want to explore nonlinear behavior in this exercise, we chose  $k = 0.10$ .

Figure 1: Estimation of time-varying coefficient model with random-walk dynamics



**Sine wave.** Finally, we use a sine function contaminated with Gaussian noise as data-generating process:

$$S_t = \sin\left(\frac{4\pi}{T}t\right) + e_t,$$

where  $t = 1, \dots, T = 61$  and  $e_t \stackrel{i.i.d.}{\sim} \mathcal{N}(0, 0.33)$ . This specification is not motivated by any physical considerations, and it is intended only to demonstrate the ability of the time-varying coefficient model to capture nonlinear behavior.

Figure 1 shows the different sink functions (black), typical trajectories (red), and the smoothed fits from 100 maximum-likelihood estimations of model (1) using the extended Kalman filter (EKF). This illustrates the flexibility of the time-varying coefficient model estimated by the EKF in capturing a wide range of nonlinear relationships.

## S2 Motivation of emission variance increase after 1996

There are three data sources for land-use-change emissions in the Global Carbon Budget file: Houghton and Nassikas (2017), Hansis et al. (2015), and Gasser et al. (2020). The change in the variance after 1996 originates from the Houghton and Nassikas (2017) and Gasser et al. (2020) data sets, and not, or at least to a much lesser degree, from the Hansis et al. (2015) data set. Although the GCB paper Friedlingstein et al. (2022) and the sources Houghton and Nassikas (2017) and Gasser et al. (2020) address uncertainty in levels very carefully, they do not discuss this particular change in the variance of first differences explicitly. Implicitly, remarks made in Section 2.2.2.3, page 460 of Houghton and Nassikas (2017) can be read such that a change in variance in first differences may be inherited from the Global Fire Emissions Database and reflects clearing of peat swamp forests in Malaysia, Papua New Guinea, and Indonesia. (“*Annual emissions from burning varied over 3 orders of magnitude.*”, p. 460 in Houghton and Nassikas (2017)) These remarks describe, however, a more gradual increase in variance from the 1980s to the present. The statistical finding of an abrupt increase in variance in 1997 can be a combination of this gradual process and the pronounced maximum in first differences of land-use change emissions in 1997, which is described in the same paper. Hence we have included a break in the variance of  $\kappa_t$  in the emission  $E^*$  updating equations (3) and (4); the increase of the variance is measured by the parameter  $s_E$  and its statistically highly significant estimate is reported in Table 1.

## S3 Approximating sink functions as linear in concentrations

### S3.1 Land sink

Bacastow and Keeling (1973) suggest that the relationship between  $S_{LND_t}$  and atmospheric CO<sub>2</sub> concentrations  $C_t$  follows

$$S_{LND_t} = \beta \log(C_t/C_{1750}), \quad (2)$$

where  $\beta$  is a constant and  $C_{1750} = 593.43$  GtC is the pre-industrial atmospheric concentration. This formula captures the fertilization effect, whereby increased CO<sub>2</sub> concentrations lead to increased net primary production of plants. Similarly to what was done in Section 2 of the paper, we can rewrite equation (2) as

$$S\_LND_t = f_{BK}^*(C_t)(C_t - C_{1750}),$$

where

$$f_{BK}^*(C_t) = \frac{\beta \log(C_t/C_{1750})}{C_t - C_{1750}}.$$

At the beginning of the sample analyzed in the paper, the atmospheric concentration is  $C_{1959} = 672.87$  GtC, while at the end of the sample it is  $C_{2020} = 879.24$  GtC. From these numbers, we find that  $f_{BK}^*(C_{1959}) = 0.0016\beta$  and  $f_{BK}^*(C_{2020}) = 0.0014\beta$ , a decrease of 12.5%. The assumption of a land sink that grows linearly in concentrations,  $k_L(C_t) = k_L$ , is thus not unreasonable on the sample. The linearity assumption was suggested already in Bacastow and Keeling (1973, p. 94), and it is discussed and applied, for example, in the context of the airborne fraction and sink rate of CO<sub>2</sub>, in Raupach et al. (2014), Raupach (2013), Gloor et al. (2010), Canadell et al. (2007), and Bennedsen et al. (2019).

An alternative expression for the fertilization effect was put forward in Gifford (1993):

$$S\_LND_t = NPP_t - NPP_{1750} = \frac{a(C_t - C_b)}{1 + b(C_t - C_b)} - \frac{a(C_{1750} - C_b)}{1 + b(C_{1750} - C_b)},$$

where NPP is net primary production and  $C_b$  is the atmospheric concentration where net primary production is zero ( $C_b = 65.9$  GtC or 31 ppm in Gifford (1993)). The parameter  $a$  plays a comparable role to the parameter  $\beta$  in the Bacastow-Keeling formula. We can rewrite this formulation as

$$S\_LND_t = f_G^*(C_t)(C_t - C_{1750}),$$

where

$$f_G^*(C_t) = \left( \frac{a(C_t - C_b)}{1 + b(C_t - C_b)} - \frac{a(C_{1750} - C_b)}{1 + b(C_{1750} - C_b)} \right) (C_t - C_{1750})^{-1}.$$

Using  $b = 0.005$ , a typical parameter value employed in Gifford (1993), along with the concentra-

tion levels given above, we find that  $f_G^*(C_{1959}) = 0.0683a$  and  $f_G^*(C_{2020}) = 0.0543a$ , a decrease of 20.5%. Thus, the Gifford formula has more curvature for typical parameter values, and the linear approximation is less accurate than for the Bacastow-Keeling specification.

Both the Bacastow-Keeling and the Gifford formulae imply that a regression of  $S\_LND$  on  $C_t/C_{1750}$  and a constant should yield estimated intercepts and regression coefficients that are equal in magnitude with opposite signs, of course up to small sample error. (For the Bacastow-Keeling formula, the first-order term decomposes into  $-\beta$  plus  $\beta C_t / C_{1750}$ , analogously for the Gifford formula.) Table 1 shows that the estimated coefficients are numerically similar in magnitude. Indeed, the null hypothesis that intercept plus slope equal zero cannot be rejected for  $S\_LND$ . The conclusion from the hypothesis test is not sensitive to whether or not a heteroskedasticity adjustment is applied.

Table 1: Simple linear regressions of the sinks series on normalized atmospheric concentrations  $C_t/C_{1750}$ . Standard errors in parentheses.  $F$  is the  $F$ -statistic for a test that intercept plus slope equal zero.  $C_{1750} = 593.43\text{GtC}$ . The Durbin-Watson statistic indicates first-order serial correlation when it deviates from the benchmark value of 2.

Series	intercept	$C_t/C_{1750}$	Durbin-Watson	$F$
S_LND	-6.72 (1.12)	7.12 (0.88)	2.02	2.37 ( $p=0.13$ )
S_OCN	-4.86 (0.24)	5.18 (0.18)	0.66	36.62 ( $p=1\text{e-}7$ )

### S3.2 Ocean sink

As in the case of the land sink, linearity of the ocean sink in atmospheric concentrations has been employed in the literature, see for example Raupach et al. (2014), Raupach (2013), Glooer et al. (2010), Canadell et al. (2007), and Bennedsen et al. (2019). For the CO<sub>2</sub> flux from atmosphere to ocean, Joos et al. (1996) and Joos et al. (2001) specify the relation

$$S\_OCN_t = k_{O,ppm}(pCO2_t^a - pCO2_t^s),$$

where  $pCO2_t^a$  and  $pCO2_t^s$  are the partial pressures of CO<sub>2</sub> in the atmosphere at sea level and in the ocean surface layer, respectively. The coefficient  $k_{O,ppm}$  determines the gas exchange between the atmosphere and the ocean surface layer. The atmospheric partial pressure at sea level is simply a linear transformation of the atmospheric CO<sub>2</sub> concentration. The partial pressure of CO<sub>2</sub> in the surface layer of the ocean is specified as

$$\begin{aligned} pCO2_t^s = & \\ & (pCO2_0^s + \delta_1 \Phi(L) S\_OCN_t + \delta_2 [\Phi(L) S\_OCN_t]^2 + \dots + \delta_5 [\Phi(L) S\_OCN_t]^5) \exp(\gamma(T_t - T_0)), \end{aligned}$$

where  $pCO2_0^s$  is initial partial pressure in the surface ocean (equal to pre-industrial atmospheric partial pressure assuming equilibrium of the pre-industrial era ocean surface layer with the atmosphere). Since dissolution of CO<sub>2</sub> in the surface ocean depends on temperature, the coefficients  $\delta_i = \delta_i(T_0)$  depend on the initial temperature  $T_0$ , and the expression in parentheses is multiplied by an exponential evaluated in the temperature difference  $T_t - T_0$  between time  $t$  and time 0, multiplied by a coefficient  $\gamma$ . The lag polynomial  $\Phi(L)$  is a time-invariant linear filter that describes the dissolution of carbon from the atmosphere in the surface ocean over time:

$$\Phi(L)S\_OCN_t = \phi_1 S\_OCN_{t-1} + \phi_2 S\_OCN_{t-2} + \dots + \phi_{t-1} S\_OCN_1.$$

We present the model for an annual sampling frequency. It is specified in Joos et al. (1996) and Joos et al. (2001) for higher resolutions as well, with different  $\Phi(L)$  filters for subannual responses, but we abstract from this due to the nature of the data. This model for the ocean sink is employed, for example, in the widely used MAGICC model (Meinshausen et al., 2011). It is clearly a highly nonlinear description of the uptake and dissolution process and how it depends on the pressure differential, the temperature, and temporal dynamics. The key features of the specification for the purposes of our statistical analysis are:

- a) After suitable unit conversions, the model can be written in the form

$$S\_OCN_t = k_{O,GtC}[C_t - C_{1750} - f(\Phi(L)S\_OCN_t)], \quad (3)$$

that is, with a leading linear term in current atmospheric CO<sub>2</sub> concentrations.

- b) When we approximate equation (3) as

$$S\_OCN_t \approx c_O + k_O C_t, \quad (4)$$

lags of  $S\_OCN_t$ , and hence lags of  $C_t$ , enter into the approximation error both linearly and nonlinearly up to fifth powers through function  $f$ . This introduces serial correlation (linear terms) and memory in higher moments (nonlinear terms). We show in Section 4 in the paper that on the data sample, this memory can be sufficiently captured with a linear first-order autoregressive filter, such that the residuals appear as Gaussian white noise.

- c) The linear specification in concentrations (4) is similar to the linearized specification for the land sink discussed above. In particular, estimating a linear regression on  $C_t/C_{1750}$ , we expect

an estimated intercept of the same magnitude as the regression coefficient, with opposite sign. Table 1 shows that the coefficients are numerically similar in magnitude, but the  $F$  test rejects the null hypothesis that their sum is zero. The conclusion does not depend on whether or not a heteroskedasticity adjustment is applied, which is the case here. The Durbin-Watson statistic in the table shows evidence for serial correlation.

## S4 State space system matrices

In this section, we define the system matrices of the state space model. We specify the  $X_i$  and  $X^E$  processes as follows.

$$X_{1,t+1} = \phi_1 X_{1,t} + \eta_{1,t+1}, \quad (5)$$

$$X_{2,t+1} = \eta_{2,t+1}, \quad (6)$$

$$X_{3,t+1} = \phi_3 X_{3,t} + \eta_{3,t+1}, \quad (7)$$

$$X_{4,t+1} = \eta_{4,t+1}, \quad (8)$$

$$X_{t+1}^E = \phi_E X_t^E + \kappa_{t+1}, \quad (9)$$

where  $\phi_{1,3,E} \in (-1, 1)$ . Defining the measurement vector as  $y_t = (C_t, E_t, S\_LND_t, S\_OCN_t)'$  and the state vector as  $\alpha_t = (C_t^*, G\_ATM_t^*, S\_LND_t^*, S\_OCN_t^*, X_{1,t}, X_{2,t}, X_{3,t}, X_{4,t}, X_t^E, E_t^*)'$ , the model can be represented as

$$\begin{aligned} y_t &= Z\alpha_t, \\ B\alpha_{t+1} &= \tilde{c} + \tilde{T}\alpha_t + \tilde{\eta}_t, \end{aligned} \quad (10)$$

where the matrix  $B$  contains the contemporary relations: G\_ATM depending on concurrent E, S\_LND, and S\_OCN, the sinks depending on concurrent C.

Pre-multiplying the state equation with  $B^{-1}$  transforms model (10) to standard state space form:

$$\begin{aligned} y_t &= Z\alpha_t, \\ \alpha_{t+1} &= c + T\alpha_t + \eta_t. \end{aligned} \quad (11)$$

Explicitly, (11) is given by the measurement equation

$$\begin{bmatrix} C_t \\ E_t \\ S\_LND_t \\ S\_OCN_t \end{bmatrix} = \begin{bmatrix} 1 & 0 & 0 & 0 & 1 & 0 & 0 & 0 & 0 & 0 \\ 0 & 0 & 0 & 0 & 0 & 0 & 0 & 1 & 1 & 0 \\ 0 & 0 & 1 & 0 & 0 & 1 & 0 & 0 & 0 & 0 \\ 0 & 0 & 0 & 1 & 0 & 0 & 1 & 0 & 0 & 0 \end{bmatrix} \begin{bmatrix} C_t^* \\ G\_ATM_t^* \\ S\_LND_t^* \\ S\_OCN_t^* \\ X_{1,t} \\ X_{2,t} \\ X_{3,t} \\ X_{4,t} \\ X_t^E \\ E_t^* \end{bmatrix}.$$

The state equation is

$$\begin{bmatrix} 1 & -1 & 0 & 0 & 0 & 0 & 0 & 0 & 0 & 0 \\ 0 & 1 & 1 & 1 & 0 & 0 & 0 & 0 & 0 & -1 \\ -\frac{\beta_1}{C_0} & 0 & 1 & 0 & 0 & 0 & 0 & 0 & 0 & 0 \\ -\frac{\beta_2}{C_0} & 0 & 0 & 1 & 0 & 0 & 0 & 0 & 0 & 0 \\ 0 & 0 & 0 & 0 & 1 & 0 & 0 & 0 & 0 & 0 \\ 0 & 0 & 0 & 0 & 0 & 1 & 0 & 0 & 0 & 0 \\ 0 & 0 & 0 & 0 & 0 & 0 & 1 & 0 & 0 & 0 \\ 0 & 0 & 0 & 0 & 0 & 0 & 0 & 1 & 0 & 0 \\ 0 & 0 & 0 & 0 & 0 & 0 & 0 & 0 & 1 & 0 \\ 0 & 0 & 0 & 0 & 0 & 0 & 0 & 0 & 0 & 1 \end{bmatrix} \begin{bmatrix} C_{t+1}^* \\ G\_ATM_{t+1}^* \\ S\_LND_{t+1}^* \\ S\_OCN_{t+1}^* \\ X_{1,t+1} \\ X_{2,t+1} \\ X_{3,t+1} \\ X_{4,t+1} \\ X_{t+1}^E \\ E_{t+1}^* \end{bmatrix} = \begin{bmatrix} 1 & 0 & 0 & 0 & 0 & 0 & 0 & 0 & 0 & 0 \\ 0 & 0 & 0 & 0 & 0 & 0 & 0 & 0 & 0 & 0 \\ 0 & 0 & 0 & 0 & 0 & 0 & 0 & 0 & 0 & 0 \\ 0 & 0 & 0 & 0 & 0 & 0 & 0 & 0 & 0 & 0 \\ 0 & 0 & 0 & 0 & 0 & \phi_1 & 0 & 0 & 0 & 0 \\ 0 & 0 & 0 & 0 & 0 & 0 & 0 & 0 & 0 & 0 \\ 0 & 0 & 0 & 0 & 0 & 0 & 0 & \phi_3 & 0 & 0 \\ 0 & 0 & 0 & 0 & 0 & 0 & 0 & 0 & 0 & 0 \\ 0 & 0 & 0 & 0 & 0 & 0 & 0 & 0 & 0 & \phi_E \\ 0 & 0 & 0 & 0 & 0 & 0 & 0 & 0 & 1 & 1 \end{bmatrix} \begin{bmatrix} C_t^* \\ G\_ATM_t^* \\ S\_LND_t^* \\ S\_OCN_t^* \\ X_{1,t} \\ X_{2,t} \\ X_{3,t} \\ X_{4,t} \\ X_t^E \\ E_t^* \end{bmatrix}$$

$$+ \begin{bmatrix} 0 \\ 0 \\ c_1 \\ c_2 \\ 0 \\ 0 \\ 0 \\ 0 \\ 0 \\ d \end{bmatrix} + \begin{bmatrix} 0 \\ 0 \\ \eta_{1,t} \\ \eta_{2,t} \\ \eta_{3,t} \\ \eta_{4,t} \\ \eta_{5,t} \\ 0 \end{bmatrix}.$$

It holds that

where

$$\beta_1^* = \frac{\beta_1}{C_0}, \quad \beta_2^* = \frac{\beta_2}{C_0}, \quad c = 1 + \beta_1^* + \beta_2^*.$$

Then,

and

$$\begin{bmatrix} \frac{1}{c} & \frac{1}{c} & \frac{-1}{c} & \frac{-1}{c} & 0 & 0 & 0 & 0 & 0 & \frac{1}{c} \\ -(\beta_1^* + \beta_2^*) & \frac{1}{c} & -1 & -1 & 0 & 0 & 0 & 0 & 0 & \frac{1}{c} \\ \frac{c}{\beta_1^*} & \frac{\beta_1^*}{c} & 1+\beta_2^* & -\beta_1^* & 0 & 0 & 0 & 0 & 0 & \frac{c}{\beta_1^*} \\ \frac{c}{\beta_2^*} & \frac{\beta_2^*}{c} & -\beta_2^* & \frac{c}{\beta_2^*} & 0 & 0 & 0 & 0 & 0 & \frac{c}{\beta_2^*} \\ 0 & 0 & 0 & 0 & 1 & 0 & 0 & 0 & 0 & 0 \\ 0 & 0 & 0 & 0 & 0 & 1 & 0 & 0 & 0 & 0 \\ 0 & 0 & 0 & 0 & 0 & 0 & 1 & 0 & 0 & 0 \\ 0 & 0 & 0 & 0 & 0 & 0 & 0 & 1 & 0 & 0 \\ 0 & 0 & 0 & 0 & 0 & 0 & 0 & 0 & 1 & 0 \\ 0 & 0 & 0 & 0 & 0 & 0 & 0 & 0 & 0 & 1 \end{bmatrix} \begin{bmatrix} 0 \\ 0 \\ 0 \\ 0 \\ \eta_{1,t} \\ \eta_{2,t} \\ \eta_{3,t} \\ \eta_{4,t} \\ \eta_{5,t} \\ 0 \end{bmatrix} = \begin{bmatrix} 0 \\ 0 \\ 0 \\ 0 \\ \eta_{1,t} \\ \eta_{2,t} \\ \eta_{3,t} \\ \eta_{4,t} \\ \eta_{5,t} \\ 0 \end{bmatrix}.$$

The covariance matrix  $Q$  of the errors  $\eta_t$  in the state equation is given by zeros except the entries in rows and columns 5 to 9, which are

$$Q[5 : 8, 5 : 8] = \begin{bmatrix} \sigma_{\eta_1}^2 & r_{12}\sigma_{\eta_1}\sigma_{\eta_2} & r_{13}\sigma_{\eta_1}\sigma_{\eta_3} & 0 & 0 \\ r_{12}\sigma_{\eta_1}\sigma_{\eta_2} & \sigma_{\eta_2}^2 & 0 & 0 & 0 \\ r_{13}\sigma_{\eta_1}\sigma_{\eta_3} & 0 & \sigma_{\eta_3}^2 & 0 & 0 \\ 0 & 0 & 0 & \sigma_{\eta_4}^2 & 0 \\ 0 & 0 & 0 & 0 & \sigma_{\kappa}^2 \end{bmatrix}.$$

## S5 Impulse Response Function

We can construct an impulse response function of atmospheric CO<sub>2</sub> concentrations with respect to emissions from the solution (18) for  $C_t^*$ . If we consider an initial pulse in emissions,  $E_0^* = \varepsilon$ , followed by zero-emissions  $E_t^* = 0$  for  $t > 0$ , the resulting equation for atmospheric concentrations at point  $t = 1$  becomes

$$C_1^* = C_0^* + E_0^* - S\_LND_1^* - S\_OCN_1^* = C_0^* + \varepsilon - S\_LND_1^* - S\_OCN_1^*,$$

so that this initial pulse can be added to the initial concentrations, which are now  $\tilde{C}_0^* = C_0^* + \varepsilon$ . The dynamics of atmospheric concentrations in the absence of emissions (for  $t > 1$ ) are given as

$$\begin{aligned} C_t^* &= C_{t-1}^* - S\_LND_t^* - S\_OCN_t^*, \\ &= C_{t-1}^* - (c_1 + c_2) - \frac{\beta_1 + \beta_2}{C_0} C_t^*, \end{aligned}$$

with solution

$$C_t^* = \delta^t \left( \tilde{C}_0^* + c \frac{\delta}{1-\delta} \right) - c \frac{\delta}{1-\delta},$$

where  $c = c_1 + c_2$ . The term  $\tilde{C}_0^* + c \frac{\delta}{1-\delta}$  measures the distance of the initial condition  $\tilde{C}_0^*$  from the limit  $-c \frac{\delta}{1-\delta}$ .

We can compute and estimate the limit given the estimated coefficients, with the caveat that we are extrapolating the behavior of the system to a zero-emissions regime, on which it was not estimated. This estimate is

$$-\hat{c} \frac{\hat{\delta}}{1-\hat{\delta}} = -(\hat{c}_1 + \hat{c}_2) \frac{\hat{\delta}}{1-\hat{\delta}} = -(-4.13 - 5.11) \frac{0.9827}{0.0173} = 524.86 \text{GtC}$$

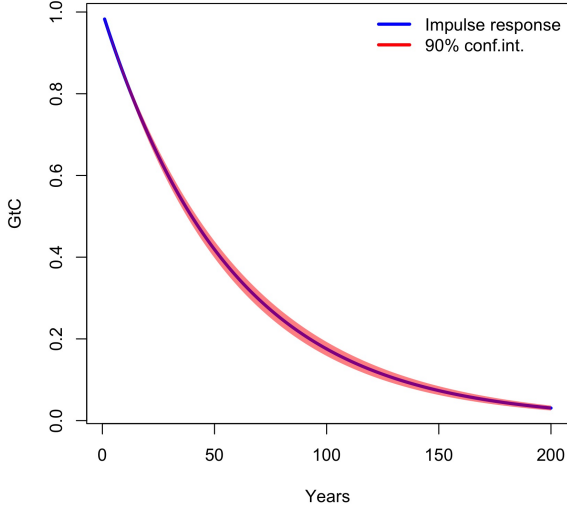
or about 246ppm. This is reasonably close to pre-industrial atmospheric concentrations  $C_{1750} = 593.4$  GtC (276ppm).

The coefficient that determines how long it takes the process to reach this limit if we were to stop emissions today is  $\delta$  and its powers, where  $\hat{\delta} = (1 + (\hat{\beta}_1 + \hat{\beta}_2)/C_{1750})^{-1} = 0.9827$ . The half-life of initial concentrations is  $-\log 2 / \log \hat{\delta} \approx 40$  years, assuming constancy of  $\beta_1$  and  $\beta_2$  under a no-emissions regime, which may not be realistic. By use of the delta-method, we can also obtain standard errors for the resulting concentrations curve, which we plot in Figure 2. Note that the implied uptake of CO<sub>2</sub> is faster than that predicted by non-statistical models (for example, Joos et al. (2013), Figure 1). The likely reason is, again, the assumption of constant coefficients  $\beta_1$  and  $\beta_2$  that retain the values estimated on the historical sample in the very different emission and concentration regimes that the impulse response scenario entails. The uncertainty bands are comparatively narrow since they only reflect parameter estimation uncertainty.

## S6 Unit root tests

The most conspicuous feature of the time series variables E\_FF, E, G\_ATM, S\_LND, and S\_OCN in Figure 1 in the paper is the upward trend, whereas the variable E\_LUC is not trending. We conduct augmented Dickey-Fuller (ADF), Phillips-Perron (PP), and Kwiatkowski, Phillips, Schmidt, and Shin (KPSS) tests for unit roots to determine the order of integration of the series and whether stationarity can be achieved by either de-trending or by differencing. We keep the notation of the original sources for each test. We emphasize that unit root tests are univariate analyses and cannot disentangle multivariate system dynamics, which are of key importance in the analysis of the GCB, as

Figure 2: Impulse response from a single GtC of emissions



discussed in Section 2 in the paper. We employ unit root analysis here to enhance our understanding of the time series properties of the variables in the GCB.

The test results are presented in Table 2: all tests do not reject the unit root hypothesis for the E\_FF time series, including the ADF test that allows for a drift term. In case of the variable E\_LUC, the tests are not unanimous: the ADF and PP tests point towards stationarity while the KPSS test rejects the stationarity hypothesis. Anthropogenic emissions E inherit the agreement of the tests on E\_FF and clearly exhibit a unit root.

The tests agree that S\_LND and S\_OCN are trend-stationary, with the Phillips-Perron test for S\_OCN as the only exception. This is at odds with the sinks' approximately linear dependence on atmospheric concentrations, which are I(1) ranging on I(2), as shown in Section 2.3.3 in the paper. However, atmospheric concentrations are very smooth compared to the sinks processes, and their curvature on the sample is so subtle that they are statistically indistinguishable from a linear trend, in particular since the variation of the sinks processes around this trend is pronounced. Since the univariate unit root tests cannot identify concentrations as the source of the trending behavior, they decide for trend-stationarity. This demonstrates that unit root tests can guide the modeling cycle in a first pass but need to be supplemented with system understanding.

Similarly, the tests agree that G\_ATM is trend-stationary. We show in Section 2.7 that concentrations  $C_t^*$  are I(1), a fact that all unit root tests agree on, and thus  $G_{ATM}^*$  is stationary. The apparent trend diagnosed here in G\_ATM is again due to the near-linearity of the smooth concentrations time series C. The linear slope of C on the sample is about 3.38 GtC/year, the slope of

anthropogenic emissions is about 0.11 GtC/year, the linear coefficients of concentrations in both S\_LND and S\_OCN are estimated to be about 0.01. Thus, using the global carbon budget equation, in G\_ATM we can expect a linear slope of about  $0.11 - (2)(0.01)(3.38) \approx 0.04$  GtC/year. The estimated linear slope of G\_ATM is about 0.06 GtC/year.

Since the emission variable  $E_t$  is modeled as the sum of a stochastic trend with drift process  $E_t^*$  and a stationary process  $X_{4t}$ , it follows that  $E_t$  is non-stationary and integrated of order one, implying that the series in first differences  $E_t - E_{t-1}$  is stationary. From the emission time series plots in Figure 1 in the paper, it appears that it is a reasonable model assumption. The unit-root tests confirm this finding: under different settings they are all significant at a 95% confidence level. BIM and SOI are found to be stationary by all tests. Differences in World GDP are found to be trend-stationary, which is expected.

Table 2: Unit root tests. Significance at the 0.01, 0.05, 0.10 levels are denoted by \*\*\*, \*\*, \*, respectively, and are according to tabulated unit root distributions, (\*\*) 0.01 significance according to standard normal.

**Augmented Dickey-Fuller test:** The ADF test regression is given by  $\Delta y_t = \alpha + \beta t + \pi y_{t-1} + \sum_{j=1}^k \gamma_j \Delta y_{t-j} + u_t$ , where we select  $k$  by Bayes Information Criterion (BIC). We test the hypothesis  $H_0 : \pi = 0$  using the t-statistic  $\hat{\tau}_\tau$  that follows a Dickey-Fuller distribution (Fuller, 1996, p. 562, 642).  $\Phi_3$  is the statistic in Table VI in Dickey and Fuller (1981).  $\hat{\tau}_\beta$  is the standard t-statistic on the trend coefficient.  $\hat{\tau}_\mu$  is a statistic from Table 10.A.2 in (Fuller, 1996, p. 642).  $\Phi_1$  is the statistic in Table IV in Dickey and Fuller (1981).

**Phillips-Perron test:** The PP test regression is given by  $y_t = \mu + \beta(t - \frac{1}{2}T) + \alpha y_{t-1} + u_t$ , where  $T$  is the sample size. Phillips and Perron (1988) define the statistic  $Z(t_\alpha)$  that follows a Dickey-Fuller distribution and is robust to serial correlation in the error term  $u_t$ . This obviates the selection of the tuning parameter  $k$  in the ADF tests. We test the hypothesis  $H_0 : \alpha = 1$  using  $Z(t_\alpha)$ . If the test rejects, the series is either stationary or trend-stationary, depending on the test of  $H_0 : \beta = 0$  using the  $Z(t_\beta)$  statistic proposed in Phillips and Perron (1988). The  $Z(t_\beta)$  statistic follows the distribution for  $\hat{\tau}_{\beta\tau}$  in Table III in Dickey and Fuller (1981).

**KPSS test:** The KPSS test considers the data-generating model  $y_t = \xi t + r_t + \varepsilon_t$ ,  $r_t = r_{t-1} + u_t$ ,  $u_t \stackrel{i.i.d.}{\sim} N(0, \sigma_u^2)$ , and  $\varepsilon_t$  stationary. The test is for  $H_0 : \sigma_u^2 = 0$ , that is, unlike the ADF and Phillips-Perron tests, here the null hypothesis is trend-stationarity. The Lagrange multiplier test statistic is proposed in Kwiatkowski et al. (1992). The asymptotic distribution for  $\xi = 0$  is a first-level Cramér-von Mises distribution, the asymptotic distribution for  $\xi \neq 0$  is a second-level Cramér-von Mises distribution. For LM(trend), the residuals  $e_j$  are from a regression on a constant and a trend, for LM(constant), on a constant only.

Series	Augmented Dickey-Fuller test			Phillips-Perron test			KPSS test		
	$\hat{\tau}_\tau$	$\Phi_3$	$\hat{\tau}_\beta$	$\hat{\tau}_\mu$	$\Phi_1$	Decision	$Z(t_\alpha)$	$Z(t_\beta)$	Decision
E_FF	-1.932 $K=1$	2.406	-1.325 $K=1$	3.639	I(1)	-1.767 stationary	-3.363* I(1)	I(1)	0.169** I(1)
E_LUC	-3.480** $K=1$	6.056* $K=1$	-1.558 $K=1$	-1.113 $K=1$	4.628* I(1)	-2.142 trend-stationary	-2.142 trend-stationary	I(1)	0.160** I(1)
E	-1.952 $K=1$	2.258	-1.113 $K=1$	4.372*** $K=1$		-7.172*** I(1)	5.370*** I(1)	trend-stationary	0.177** I(1)
G_ATM	-5.660*** $K=1$					-0.322 trend-stationary	-0.322 trend-stationary		0.060 trend-stationary
C	0.283 $K=1$	10.951*** $K=1$	4.793*** $K=1$	3.524*** $K=1$		-7.911*** trend-stationary	4.692*** trend-stationary		1.336*** I(1)
S_LND	-6.960*** $K=1$					-3.267* stationary	3.290* stationary		0.386*** I(1)
S_OCN	-3.458** $K=1$					-5.507*** stationary	-1.571 stationary		0.051 0.240
BIM	-4.635*** $K=1$		-0.645			-5.938*** stationary	-0.181 stationary		1.253*** stationary
SOI	-5.082*** $K=1$	0.285				-4.732** trend-stationary	-2.896 stationary		0.097 0.106
GGDP	-4.889*** $K=1$		-2.777*** $K=1$						0.111 0.084 0.771*** trend-stationary

## S7 Monte Carlo simulation of the linear model

To validate the maximum likelihood estimation procedure for the unknown parameters in the linear model, we conduct a Monte Carlo simulation study. We consider the linear model as set out in Section 2.6 in the paper. Given this model specification and with a choice of data-generating (“true”) parameter values, we simulate data for the four “observed” time series variables  $\{C_t, S\_LND_t, S\_OCN_t, E_t\}$  from a basic version of our model that does not feature dependency and thus simulations of  $\Delta ECON$  or  $ENSO$ . Emissions are simulated as random walks with constant drift  $d > 0$ . We notice that before we can simulate the four “observed” time series, we first need to simulate paths for the “unobserved” variables  $C_t^*$  and  $E_t^*$  from their dynamic model equations in Section 2.6 of the paper. Our Monte Carlo study consists of  $M$  simulations. For each simulation, we estimate the parameters in the basic model using the set of the four simulated time series. In this way, we obtain a collection of  $M$  estimates for the parameter vector. We assess the accuracy of the estimates by comparing the estimated parameter values with their corresponding “true” values. In Table 3 we report the sample bias and sample standard error for all parameters. Our Monte Carlo study is based on  $M = 1,000$  simulations and on three different time series lengths  $T = 30$ ,  $T = 60$  and  $T = 120$ . In the empirical study, we have  $T = 62$ .

First, we study the performance of the maximum likelihood estimation method for the correct model specification: we consider the same model for simulation as for estimation. The “true” parameter values in this Monte Carlo study are chosen such that they resemble the estimated parameter values in the empirical study of Section 4 in the paper. Given that the model is linear and Gaussian, and given that the exact maximum likelihood estimation method has generally good finite sample properties, we expect a good performance overall. However, for the small sample cases (e.g.  $T = 30$  and  $T = 60$ ), it is possible that the variances for latent components such as  $X_{i,t}$ , for  $i = 1, \dots, 4$ , can be subject to the “pile-up” problem, which refers to the case that a high number of estimated variances are equal to the boundary value of zero, see the discussions in Shephard (1993) and Stock and Watson (1996). In particular, the “true” variance for  $X_{4,t}$  equals the relatively small value of 0.001 and a strong pile-up is evidenced by the relatively large bias and large standard error, especially for the two smaller sample sizes. All other model parameters show good performances with small biases and small standard errors. The bias is measured as the sample mean over the set of  $M$  parameter estimates, minus the “true” parameter value. The standard error is obtained from the corresponding sample variance.

Next, we extend the Monte Carlo study and assess the estimation accuracy in cases where the

**Table 3: Results of Monte Carlo Study.** Sample mean bias and sample standard errors (in parentheses) are reported for the parameter estimates based on  $M = 1,000$  simulations from the basic model specification in Section 2.6 of the paper, where  $X_{2,t}$ ,  $X_{4,t}$  and  $X_t^E$  are Gaussian noise variables with zero mean and variance  $\sigma_{\eta_2}^2$ ,  $\sigma_{\eta_4}^2$  and  $\sigma_{\eta_5}^2$ , respectively, where  $X_{1,t}$  and  $X_{3,t}$  are first-order autoregressive processes with zero mean, variance  $\sigma_{\eta_1}^2$  and  $\sigma_{\eta_3}^2$ , and autoregressive coefficient  $\phi_1$  and  $\phi_3$ , respectively, and where  $r_{12}$  and  $r_{13}$  are the correlations for the pairs  $(X_{1,t}, X_{2,t})$  and  $(X_{1,t}, X_{3,t})$ , respectively. The parameter values are selected to be close to those obtained in the empirical study of Section 4 in the paper. Results are presented for different model specifications that are described in this section. The columns denoted “set  $x = 0$ ” refer to misspecifications of the estimated model where  $x$  is ignored in the estimation. The columns denoted “br  $x$ ” refer to data-generating processes with breaks in  $x$ , as explained in this section.

true par.	correct spec.	set $\beta_{1,2} = 0$	set $\phi_{1,3} = 0$	set $r_{12,13} = 0$	br $G_{ATM}$	br $\text{Var}(\eta_t)$
$T = 30$						
$c_1$	-7.22	.2672 (.6.17)	3.664 (136.)	.0356 (.965)	-.1726 (8.54)	0.137 (6.92)
$c_2$	-4.93	.1153 (4.10)	2.887 (107.)	-.0192 (.440)	-.1531 (6.32)	0.062 (5.23)
$\beta_1$	7.0	-.0268 (1.00)	—	-.0374 (.938)	-.0134 (.990)	-.026 (.921)
$\beta_2$	5.5	.0208 (.456)	—	.0187 (.423)	.0236 (.449)	0.019 (.415)
$d$	0.14	-.0009 (.033)	-.0009 (.033)	-.0009 (.033)	-.0009 (.033)	0.061 (.033)
$\phi_1$	0.8	-.0813 (.167)	-.0261 (.150)	—	-.0795 (.159)	-.081 (.168)
$\phi_3$	0.7	-.1124 (.184)	-.0445 (.168)	—	-.1120 (.178)	-.112 (.184)
$\sigma_{\eta_1}^2$	0.90	-.0469 (.265)	-.0035 (.271)	-.0208 (.249)	-.0641 (.229)	-.052 (.266)
$\sigma_{\eta_2}^2$	0.70	-.0158 (.189)	-.0062 (.187)	-.0159 (.188)	-.0238 (.165)	-.016 (.188)
$\sigma_{\eta_3}^2$	0.01	-.0007 (.003)	-.0003 (.003)	-.0003 (.003)	-.0008 (.003)	-.001 (.003)
$\sigma_{\eta_4}^2$	0.001	.0018 (.004)	.0019 (.004)	.0018 (.004)	.0018 (.004)	0.006 (.011)
$\sigma_{\kappa}^2$	0.03	-.0042 (.011)	-.0042 (.011)	-.0042 (.011)	-.0042 (.011)	0.096 (.030)
$r_{12}$	-0.65	.0061 (.117)	.0043 (.113)	.0140 (.114)	—	0.004 (.118)
$r_{13}$	-0.15	-.0096 (.162)	-.0086 (.157)	-.0007 (.150)	—	-.011 (.162)
$T = 60$						
$c_1$	-7.22	-.0285 (.446)	-.0099 (.216)	-.0181 (.335)	-.0043 (.758)	-.0214 (.377)
$c_2$	-4.93	.0005 (.317)	-.0093 (.167)	.0029 (.208)	.0179 (.549)	.0041 (.256)
$\beta_1$	7.0	.0194 (.287)	—	.0157 (.271)	.0186 (.286)	.0179 (.264)
$\beta_2$	5.5	-.0048 (.178)	—	-.0028 (.167)	-.0047 (.177)	-.0041 (.164)
$d$	0.14	-.0006 (.023)	-.0006 (.023)	-.0006 (.023)	-.0006 (.023)	.0293 (.023)
$\phi_1$	0.8	-.0359 (.091)	-.0111 (.085)	—	-.0356 (.089)	-.0361 (.091)
$\phi_3$	0.7	-.0474 (.112)	-.0171 (.103)	—	-.0457 (.111)	-.0474 (.112)
$\sigma_{\eta_1}^2$	0.90	-.0276 (.168)	-.0104 (.168)	-.0152 (.167)	-.0387 (.145)	-.0296 (.168)
$\sigma_{\eta_2}^2$	0.70	-.0076 (.127)	-.0049 (.127)	-.0069 (.128)	-.0150 (.114)	-.0076 (.127)
$\sigma_{\eta_3}^2$	0.01	-.0003 (.002)	-.0002 (.002)	-.0002 (.002)	-.0003 (.002)	-.0003 (.002)
$\sigma_{\eta_4}^2$	0.001	.0014 (.003)	.0015 (.003)	.0014 (.003)	.0014 (.003)	.0028 (.005)
$\sigma_{\kappa}^2$	0.03	-.0027 (.008)	-.0028 (.008)	-.0028 (.008)	-.0027 (.008)	.0464 (.015)
$r_{12}$	-0.65	-.0026 (.077)	-.0010 (.077)	.0017 (.077)	—	-.0034 (.077)
$r_{13}$	-0.15	-.0008 (.103)	-.0004 (.102)	.0008 (.099)	—	-.0012 (.103)
$T = 120$						
$c_1$	-7.22	-.0034 (.123)	-.0008 (.030)	-.0045 (.126)	-.0036 (.129)	-.0029 (.123)
$c_2$	-4.93	-.0013 (.107)	.0005 (.027)	-.0003 (.102)	-.0018 (.106)	-.0014 (.102)
$\beta_1$	7.0	.0017 (.079)	—	.0021 (.076)	.0017 (.078)	.0014 (.074)
$\beta_2$	5.5	.0009 (.066)	—	.0005 (.062)	.0013 (.065)	.0010 (.062)
$d$	0.14	-.0003 (.016)	-.0003 (.016)	-.0003 (.016)	-.0003 (.016)	.0144 (.016)
$\phi_1$	0.8	-.0173 (.050)	-.0075 (.048)	—	-.0169 (.049)	-.0176 (.050)
$\phi_3$	0.7	-.0242 (.073)	-.0113 (.068)	—	-.0244 (.072)	-.0243 (.073)
$\sigma_{\eta_1}^2$	0.90	-.0090 (.116)	-.0024 (.117)	-.0033 (.115)	-.0131 (.103)	-.0097 (.116)
$\sigma_{\eta_2}^2$	0.70	.0041 (.089)	.0052 (.088)	.0042 (.088)	.0011 (.080)	.0041 (.089)
$\sigma_{\eta_3}^2$	0.01	-.0002 (.001)	-.0001 (.001)	-.0001 (.001)	-.0002 (.001)	-.0002 (.001)
$\sigma_{\eta_4}^2$	0.001	.0007 (.002)	.0008 (.002)	.0007 (.002)	.0007 (.002)	.0012 (.003)
$\sigma_{\kappa}^2$	0.03	-.0015 (.006)	-.0016 (.006)	-.0015 (.006)	-.0015 (.006)	.0227 (.008)
$r_{12}$	-0.65	-.0008 (.054)	.0002 (.054)	.0008 (.053)	—	-.0010 (.053)
$r_{13}$	-0.15	.0005 (.069)	.0004 (.069)	.0013 (.069)	—	.0004 (.069)

“true” model for the data generating process (DGP) and the model for estimation are different in certain ways. We start by considering cases where we set particular values for the  $\beta$ ,  $\phi$  and  $r_{ij}$  parameters in the DGP. However, during the subsequent estimation process, we restrict a particular set of parameters to zero, as if they are not present in the model. The remaining parameters are estimated as usual. We expect that the estimation of the other parameters will be affected in this erroneous setting: the estimates of the remaining parameters are subject to the incomplete model specification. The results in Table 3 confirm that model misspecification affects the estimation accuracy, especially when sample sizes are smaller. However, the model is sufficiently flexible to provide an overall good fit at the cost of increased inaccuracies in the estimation of related parameters.

Finally, we also present results for cases where the DGP is distorted. We consider the case of a structural break in the growth term in  $C_t^*$ , located in the middle of the time series and specified as a one-off change (dummy) in  $G\_ATM_t$  of 10 units. In another case we distort the DGP in the middle of the time series with a change in the variance of  $X_{i,t}$  for  $i = 1, \dots, 4$ ; in the second half of the time series, all variances are multiplied by 10. For these additional two misspecification cases, the parameters are estimated using the original model specification (ignoring the breaks). These estimation results are also presented in the last two columns of Table 3. The reported biases for these cases show that the break in variance leads to more severe distortions in estimation accuracy for all measurement variances and to some extent also for the  $\beta$  coefficients. The break in the growth term has most impact on the estimation accuracy for the growth term coefficient  $d$  itself, which is to be expected. Other parameter estimates are not heavily affected by the severe breaks in the DGP. This last point provides some evidence of our flexible and robust modeling framework.

## S8 Estimation results for the nonlinear model

In this section we report the full set of estimation results for the nonlinear model specified in Sections 2 (general specification), 2.4 and 2.5 (state space representation), and 4.1 (estimation results) in the paper. Table 4 shows the parameter estimates obtained from maximizing the likelihood function by way of the Extended Kalman filter. The estimates are numerically similar to those from the linear model in Table 1 in the paper. Table 5 shows the residual diagnostics. Figure 4 presents the smoothed state processes as obtained from the extended Kalman smoother. As can be seen, the model describes the data well: There is no remaining serial correlation in the residuals and no evidence of non-normality.

Table 4: Parameter estimates. std err: standard error

	estimate	std err			
$c_1$	-4.286	0.620	$\sigma_\kappa^2$	0.011	0.003
$c_2$	-5.137	0.395	$\sigma_1^2$	0.641	0.122
$\beta_3$	0.432	0.078	$\sigma_2^2$	0.446	0.083
$\beta_4$	-0.065	0.015	$\sigma_3^2$	0.008	0.001
$\beta_6$	0.421	0.091	$\sigma_{\beta_1}^2$	1.1e-10	2.4e-10
$\beta_7$	-2.239	0.685	$\sigma_{\beta_2}^2$	7e-10	2.7e-7
$\beta_8$	-0.174	0.100	$\sigma_{\beta_5}^2$	1.8e-6	5.4e-4
$\phi_E$	0.281	0.161	$r_{12}$	-0.628	0.085
$\phi_1$	0.750	0.094			
$\phi_3$	0.684	0.101			
$s_E$	2.329	0.438			

Table 5: Residual diagnostics on standardized residuals. std dev: standard deviation, skew: skewness, kurt: kurtosis, LB(1) Ljung-Box test statistic for first-order autocorrelation, JB: Jarque-Bera test for normality, DW: Durbin-Watson statistic, \*\*\* significant at 0.01-level, \*\* significant at 0.05-level, \* significant at 0.10-level.

Residual	mean	std dev	skew	kurt	LB(1)	JB	DW
C	-0.097	1.027	-0.133	2.383	1.246	1.166	1.676
E	0.230	0.990	-0.368	3.949	0.105	3.727	1.892
S_LND	0.125	0.985	-0.038	2.554	1.736	0.529	2.327
S_OCN	0.091	0.973	0.115	3.302	0.023	0.374	1.944

Figure 3: Estimates of the time-varying parameters and 95% confidence bands, from Extended Kalman Filter and Smoother.

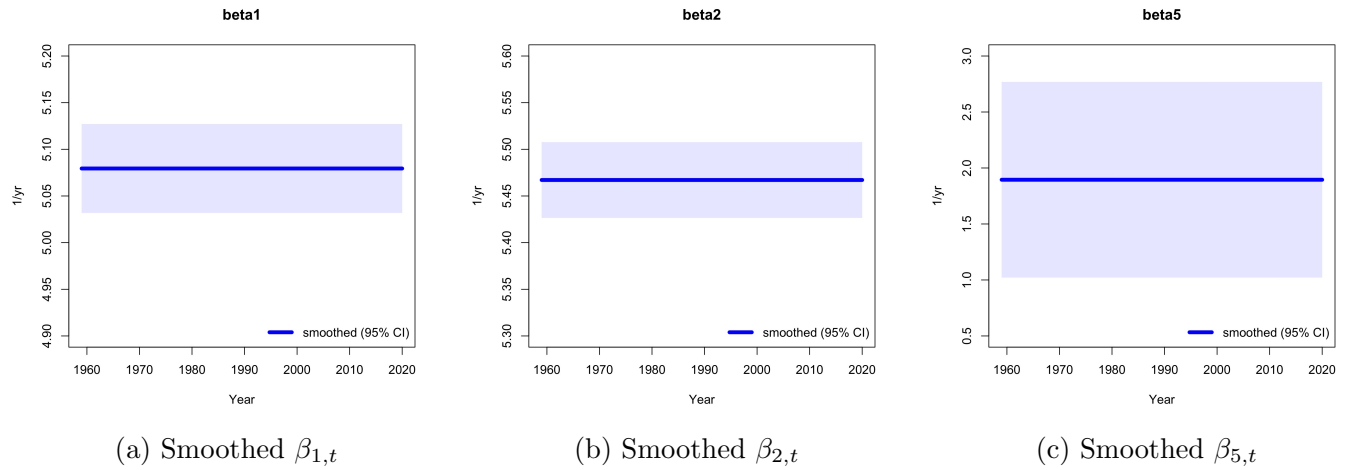
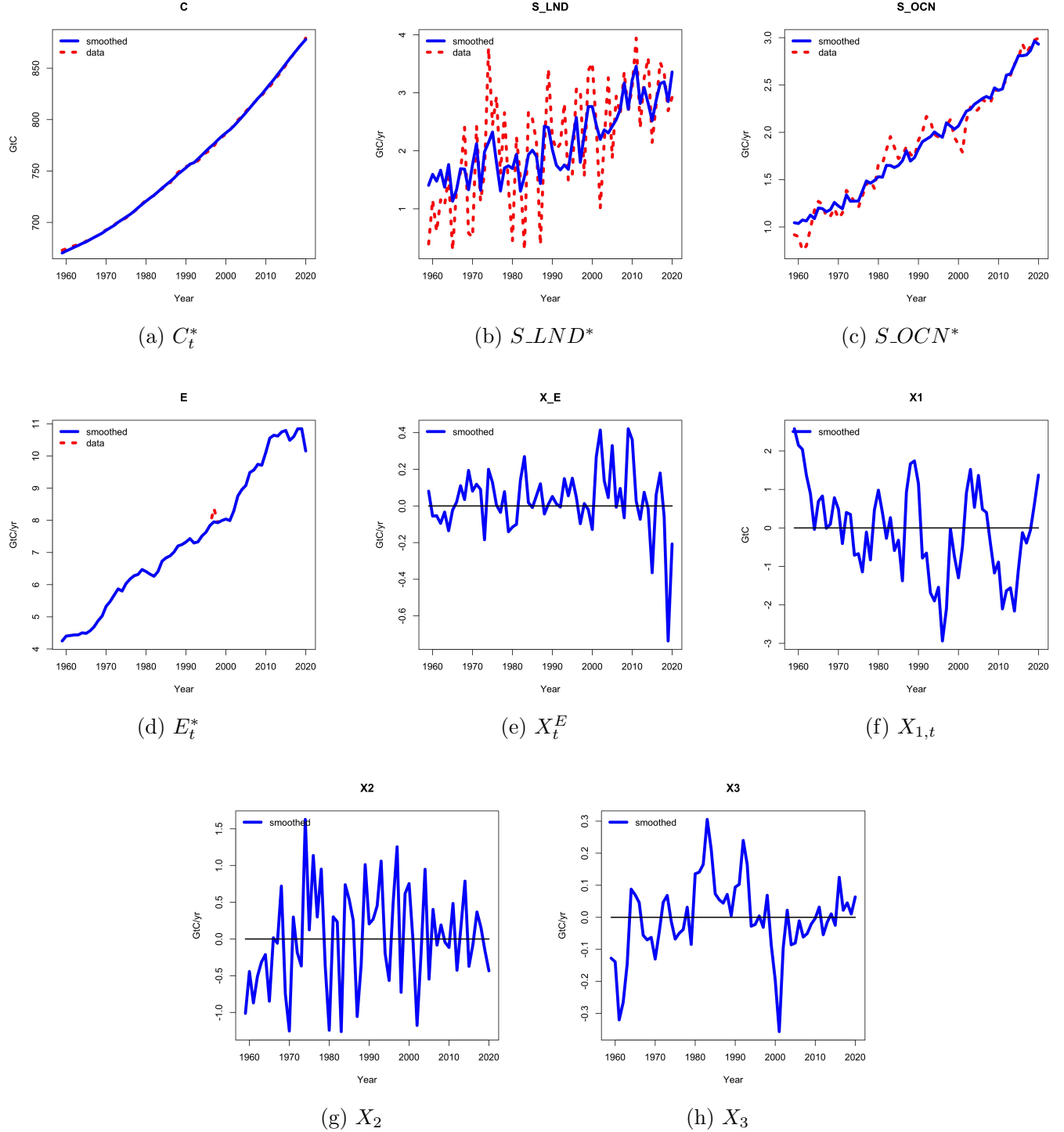


Figure 4: Smoothed states from the EKF estimation of the nonlinear model. Shown are the smoothed processes according to the recursions in Durbin and Koopman (2012, page 237).



## S9 Validation

We conduct a validation exercise on the last 10 years of the sample, that is, the validation subsample extends from 2011 to 2020. The parameters are estimated for the period 1959–2010. Using the estimated parameters and the values of  $\Delta \log GDP$  and  $SOI$  for the validation sample 2011–2020, the implied values of the system are computed for these 10 years. This results in implied values both for the measurement and for the state variables.

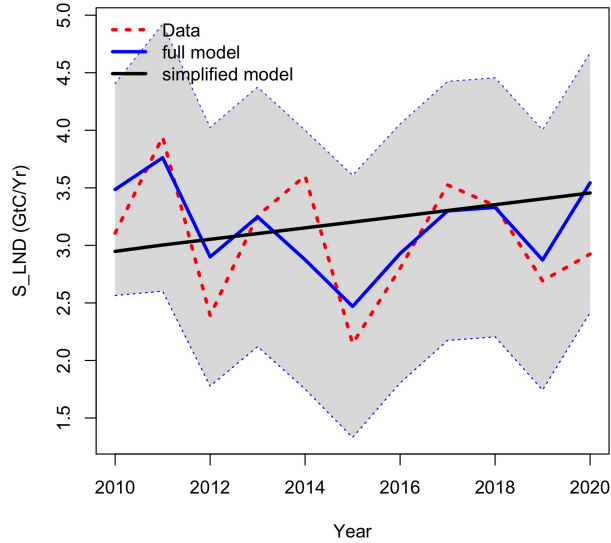
Figure 5 shows the results for the four variables S\_LND, S\_OCN, E, and G\_ATM\*. Note that the first three variables are in the measurement equation while G\_ATM\* is a state variable. We have chosen to present G\_ATM\* instead of C because there are more interesting dynamics in changes of C, and the differences between the models are easier to distinguish than in levels of C. For comparison, a simplified model that has no dependency of the sinks on SOI and no dependency of emissions E on World GDP was also validated. The point-wise 90% confidence bands are based on the full model specification.

In panels [a] to [c], the benchmarks all lie within the point-wise 90% confidence bands. For G\_ATM\*, some data points falls outside the confidence bands. Note, however, that confidence bands for state processes should not actually be compared against data points but against the estimated state process given the whole sample. This is plotted in the dashed green curve, which does fall within the confidence bands. In summary, the validation exercise shows that the model provides a good statistical description of the GCB data. On a validation sample of 10 years, it can generate implied values and confidence bands from parameters estimated on the first 50 years and from data on  $\Delta \log GDP$  and on  $SOI$  such that the data and the smoothed states obtained from the full sample lie reasonably within confidence bounds.

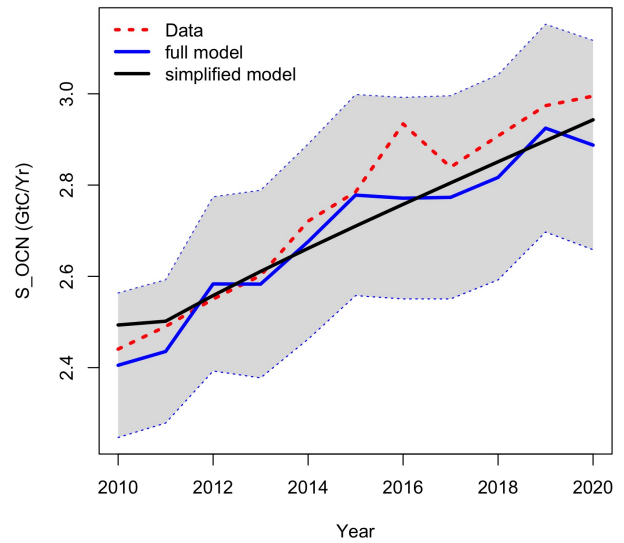
## S10 Forecast model for Southern Oscillation Index

The forecast model for monthly data on the Southern Oscillation Index (SOI) covering the period Jan-1866 to Aug-2021, obtained from Climatic Research Unit (2021) and Ropelewski and Jones (1987), is a basic structural time series model as outlined in (Durbin and Koopman, 2012, Section

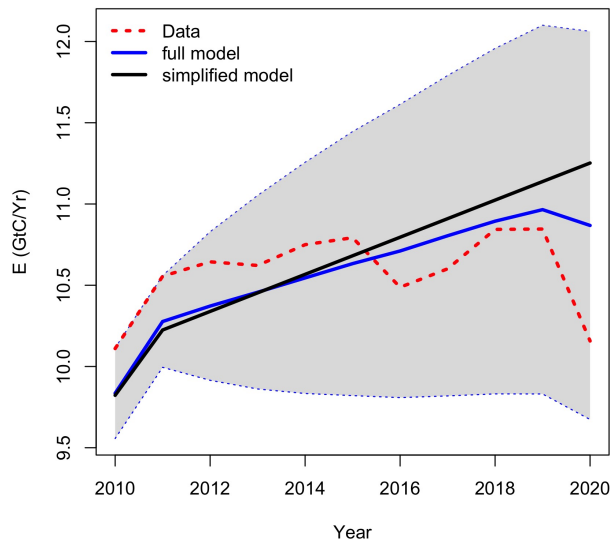
Figure 5: Validation exercise on subsample 2011–2020



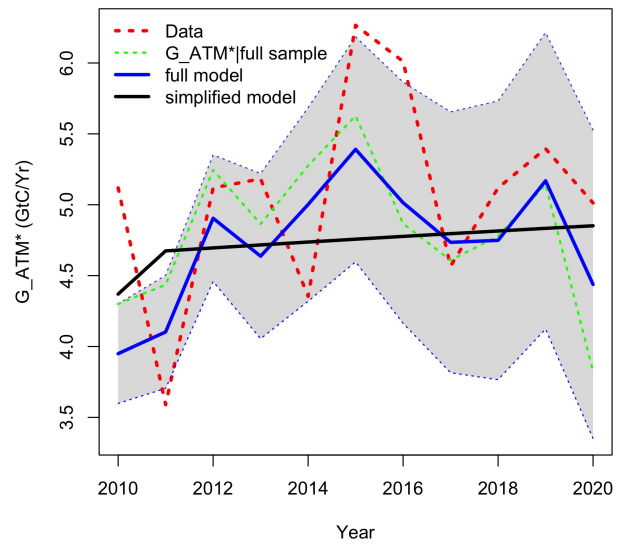
(a)  $S_{LND}$



(b)  $S_{OCN}$



(c)  $E$



(d)  $G_{ATM^*}$

3.2). The model is

$$SOI_t = \psi_t + \sum_{j=1}^6 \gamma_{j,t} + \varepsilon_t, \quad (12)$$

$$\varepsilon_t = \phi \varepsilon_{t-1} + \eta_t,$$

where  $\psi_t$  is a cycle component defined below,  $\eta_t \sim N(0, \sigma_\eta^2)$ , and  $|\phi| < 1$ . The monthly seasonal component is defined as

$$\gamma_{j,t+1} = \gamma_{j,t} \cos \lambda_j t + \gamma_{j,t}^* \sin \lambda_j t, \quad (13)$$

$$\gamma_{j,t+1}^* = -\gamma_{j,t} \sin \lambda_j t + \gamma_{j,t}^* \cos \lambda_j t, \quad (14)$$

and

$$\lambda_j = \frac{2\pi j}{12}.$$

A chi-square test for seasonality strongly rejects the null of no seasonality (30.586, with  $p$ -value 0.001). Specifying a stochastic version of the seasonal component, where equation (13) contains a random error variable, resulted in an estimated variance indistinguishable from zero, and thus the deterministic form displayed above was adopted here.

The cycle component  $\psi_t$  is defined as  $\psi_t = \psi_t^{(2)}$ , where

$$\begin{bmatrix} \psi_{t+1}^{(j)} \\ \psi_{t+1}^{*(j)} \end{bmatrix} = \begin{bmatrix} \cos \lambda & \sin \lambda \\ -\sin \lambda & \cos \lambda \end{bmatrix} \begin{bmatrix} \psi_t^{(j)} \\ \psi_t^{*(j)} \end{bmatrix} + \begin{bmatrix} \psi_t^{(j-1)} \\ \psi_t^{*(j-1)} \end{bmatrix}, \quad j = 1, 2,$$

with

$$\psi_t^{(0)} = \kappa_t \sim N(0, \sigma_\kappa^2) \quad \text{and} \quad \psi_t^{*(0)} = \kappa_t^* \sim N(0, \sigma_\kappa^2).$$

This is a second-order stochastic trigonometric cycle component with period  $2\pi/\lambda$  (Azevedo et al., 2006). The frequency is estimated as  $\hat{\lambda} = 0.129$ , translating to an estimated period of 48.8 months or about 4 years.

Including a local linear form of a trend and intercept term in (12) in addition to the AR-error and the seasonal structure,

$$\mu_t = \mu_{t-1} + \nu_{t-1} + \xi_{t-1}, \quad \xi_t \sim N(0, \sigma_\xi^2),$$

$$\nu_t = \nu_{t-1} + \zeta_{t-1}, \quad \zeta_t \sim N(0, \sigma_\zeta^2),$$

resulted in estimated variances  $\sigma_\xi^2$  and  $\sigma_\zeta^2$  indistinguishable from zero, and thus the deterministic form  $\mu + \nu t$  was tested next. The estimation resulted in insignificant coefficients  $\mu$  and  $\nu$ , consistent with the cyclical nature of El-Niño and La-Niña phases, and so the specification (12) with cycle, season, and AR(1) error was chosen.

Figure 6 shows the SOI data in the upper left panel, the smoothed cycle component  $\mathbb{E}(\hat{\psi}_t | Y_T)$  in the upper right panel, the smoothed seasonal component  $\mathbb{E}(\sum_{j=1}^6 \hat{\gamma}_{j,t} | Y_T)$  in the middle left panel, the smoothed AR(1) component  $\mathbb{E}(\hat{\varepsilon}_t | Y_T)$  in the middle right panel, and the smoothed residual  $\mathbb{E}(\hat{\eta}_t | Y_T)$  in the lower left panel. Here,  $Y_T$  is the data on the entire sample.

Figure 6: Fitted forecast model for SOI

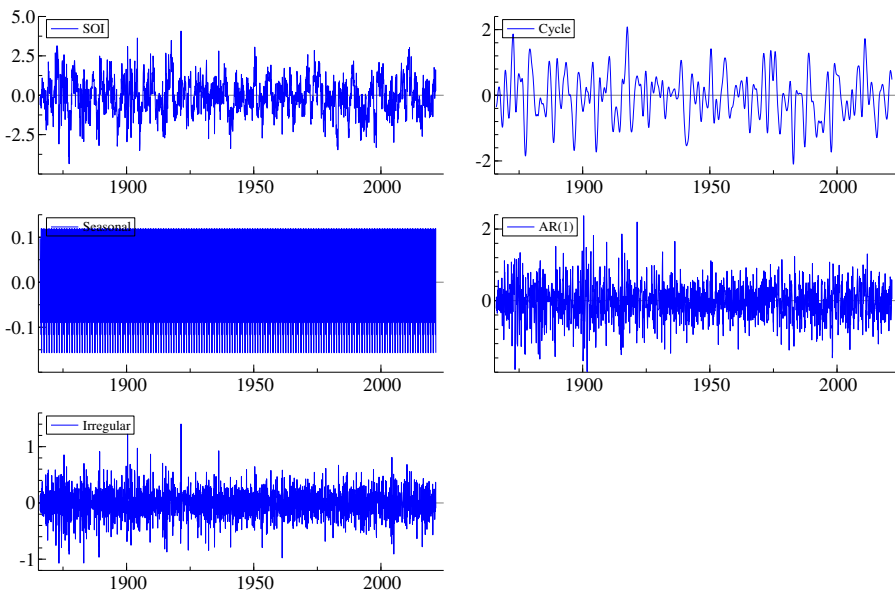


Figure 7 shows the standardized residuals from the one-step-ahead prediction in the upper left panel, the estimated sample autocorrelation function of the residuals in the upper right panel, a smoothed periodogram of the residuals in the bottom left and a histogram of the residuals in the bottom right panel.

The Durbin-Watson statistic of the residuals is 2.00; the  $R^2$  of the regression is 0.26. The Ljung-Box statistics for the first 12 lags of residuals are not significant at the 95% confidence level, despite the high number of observations ( $T = 1868$ ).

The forecast values for Sep-2021 through Dec-2023 are shown in Table 6. These forecast values were used to produce the annual forecasts of SOI used in the forecast of the global carbon budget system in Section 5.1 in the paper. These annual forecasts are the averages of the monthly values and are 0.558 for 2021, -0.081 for 2022, and -0.130 for 2023.

Figure 7: Residuals from forecast model for SOI

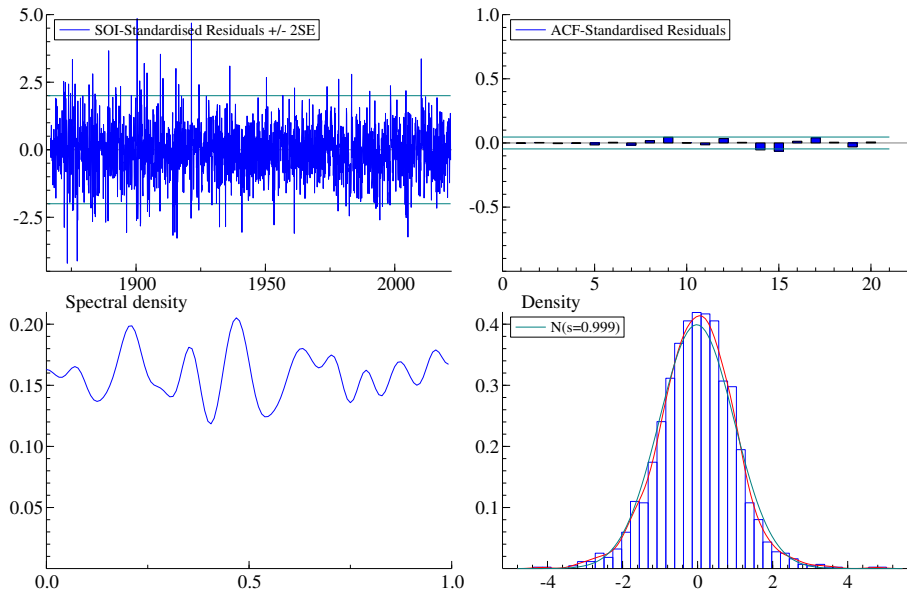


Figure 8: Forecasts for SOI

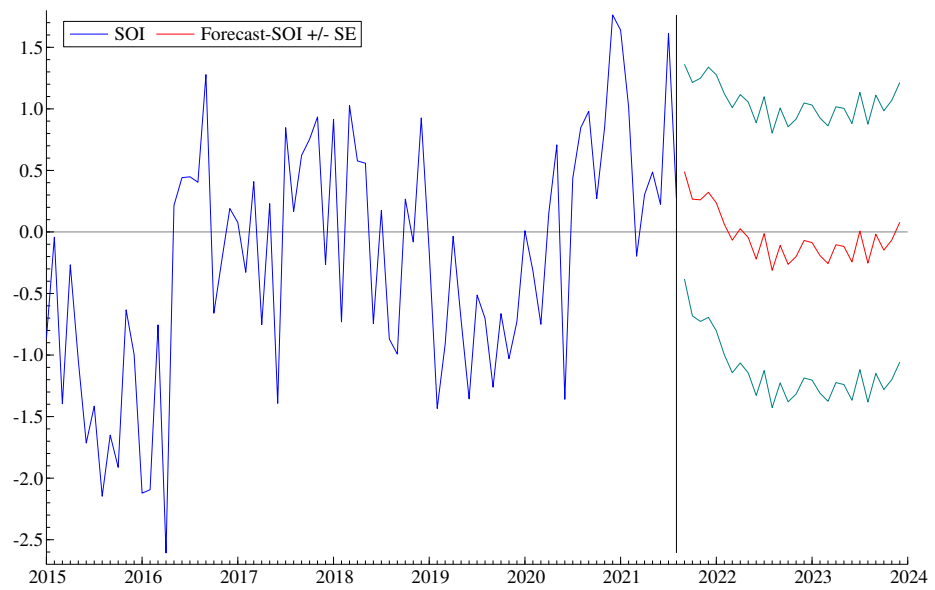


Table 6: Forecasts of SOI Aug-2020 through Dec-2021. Numbers in italics are observations.

Jan 2021	<i>1.64</i>	Jan 2022	0.236	Jan 2023	-0.086
Feb 2021	<i>1.017</i>	Feb 2022	0.063	Feb 2023	-0.192
Mar 2021	<i>-0.197</i>	Mar 2022	-0.067	Mar 2023	-0.257
Apr 2021	<i>0.303</i>	Apr 2022	0.026	Apr 2023	-0.103
May 2021	<i>0.487</i>	May 2022	-0.045	May 2023	-0.118
Jun 2021	<i>0.224</i>	Jun 2022	-0.220	Jun 2023	-0.243
Jul 2021	<i>1.614</i>	Jul 2022	-0.014	Jul 2023	0.008
Aug 2021	<i>0.273</i>	Aug 2022	-0.312	Aug 2023	-0.253
Sep 2021	0.490	Sep 2022	-0.109	Sep 2023	-0.019
Oct 2021	0.267	Oct 2022	-0.263	Oct 2023	-0.147
Nov 2021	0.261	Nov 2022	-0.200	Nov 2023	-0.065
Dec 2021	0.322	Dec 2022	-0.069	Dec 2023	-0.079
2021	0.558	2022	-0.081	2023	-0.130

## References

- Azevedo, J., Koopman, S., and Rua, A. (2006). Tracking the Business Cycle of the Euro Area. *Journal of Business and Economic Statistics*, 24:278–290.
- Bacastow, R. and Keeling, C. D. (1973). Atmospheric carbon dioxide and radiocarbon in the natural cycle: II. changes from A. D. 1700 to 2070 as deduced from a geochemical model. In *Carbon and the biosphere conference proceedings; Upton, New York, USA*, pages 86–135. Brookhaven Symposia in Biology.
- Bennedsen, M., Hillebrand, E., and Koopman, S. (2019). Trend analysis of the airborne fraction and sink rate of anthropogenically released CO<sub>2</sub>. *Biogeosciences*, 16(18):3651–3663.
- Canadell, J. G., Pataki, D. E., Gifford, R., Houghton, R. A., Luo, Y., Raupach, M. R., Smith, P., and Steffen, W. (2007). Saturation of the terrestrial carbon sink. In *Terrestrial ecosystems in a changing world*, pages 59–78. Springer.
- Climatic Research Unit (2021). University of East Anglia. Southern Oscillation Index. <https://crudata.uea.ac.uk/cru/data/soi/>. Accessed: 2020-02-15.
- Dickey, D. and Fuller, W. (1981). Likelihood Ratio Statistics for Autoregressive Time Series with a Unit Root. *Econometrica*, 49(4):1057–1072.
- Durbin, J. and Koopman, S. J. (2012). *Time series analysis by state space methods*. Oxford University Press, 2nd edition.
- Friedlingstein, P., Jones, M. W., and et al. (2022). Global Carbon Budget 2021. *Earth System Science Data*, 14:1917–2005.
- Fuller, W. (1996). *Introduction to Statistical Time Series*. John Wiley & Sons.

- Gasser, T., Crepin, L., Quilcaillie, Y., Houghton, R. A., Ciais, P., and Obersteiner, M. (2020). Historical CO<sub>2</sub> emissions from land use and land cover change and their uncertainty. *Biogeosciences*, 17(15):4075–4101.
- Gifford, R. (1993). Implications of CO<sub>2</sub> effects on vegetation for the global carbon budget. In Heimann, M., editor, *The global carbon cycle*, pages 159–199. Springer.
- Gloor, M., Sarmienti, J. L., and Gruber, N. (2010). What can be learned about carbon cycle climate feedbacks from the CO<sub>2</sub> airborne fraction? *Atmospheric Chemistry and Physics*, 10:7739 – 7751.
- Hansis, E., Davis, S., and Pongratz, J. (2015). Relevance of methodological choices for accounting of land use change carbon fluxes. *Global Biogeochemical Cycles*, 29(8):1230–1246.
- Houghton, R. and Nassikas, A. (2017). Global and regional fluxes of carbon from land use and land cover change 1850–2015. *Global Biogeochemical Cycles*, 31(3):456–472.
- Joos, F., Bruno, M., Fink, R., Siegenthaler, U., Stocker, T., Le Quere, C., and Sarmiento, J. (1996). An efficient and accurate representation of complex oceanic and biospheric models of anthropogenic carbon uptake. *Tellus B*, 48(3):397–417.
- Joos, F., Prentice, I., Sitch, S., Meyer, R., Hooss, G., Plattner, G.-K., Gerber, S., and Hasselmann, K. (2001). Global warming feedbacks on terrestrial carbon uptake under the intergovernmental panel on climate change (IPCC) emission scenarios. *Global Biogeochemical Cycles*, 15(4):891–907.
- Joos, F., Roth, R., Fuglestvedt, J. S., Peters, G. P., Enting, I. G., von Bloh, W., Brovkin, V., Burke, E. J., Eby, M., Edwards, N. R., Friedrich, T., Frölicher, T. L., Halloran, P. R., Holden, P. B., Jones, C., Kleinen, T., Mackenzie, F. T., Matsumoto, K., Meinshausen, M., Plattner, G.-K., Reisinger, A., Segschneider, J., Shaffer, G., Steinacher, M., Strassmann, K., Tanaka, K., Timmermann, A., and Weaver, A. J. (2013). Carbon dioxide and climate impulse response functions for the computation of greenhouse gas metrics: a multi-model analysis. *Atmospheric Chemistry and Physics*, 13(5):2793–2825.
- Kwiatkowski, D., Phillips, P., Schmidt, P., and Shin, Y. (1992). Testing the null hypothesis of stationarity against the alternative of a unit root: How sure are we that economic time series have a unit root? *Journal of Econometrics*, 54(1-3):159–178.
- Meinshausen, M., Raper, S., and Wigley, T. (2011). Emulating coupled atmosphere-ocean and carbon cycle models with a simpler model, magicc6—part 1: Model description and calibration. *Atmospheric Chemistry and Physics*, 11(4):1417–1456.
- Phillips, P. and Perron, P. (1988). Testing for a unit root in time series regression. *Biometrika*, 75(2):335–346.
- Raupach, M. R. (2013). The exponential eigenmodes of the carbon-climate system, and their implications for ratios of responses to forcings. *Earth System Dynamics*, 4:31 – 49.
- Raupach, M. R., Gloor, M., Sarmiento, J. L., Canadell, J. G., Frölicher, T. L., Gasser, T., Houghton, R. A., Le Quéré, C., and Trudinger, C. M. (2014). The declining uptake rate of atmospheric CO<sub>2</sub> by land and ocean sinks. *Biogeosciences*, 11(13):3453–3475.

- Ropelewski, C. and Jones, P. (1987). An extension of the Tahiti-Darwin Southern Oscillation Index. *Monthly Weather Review*, 115:2161–2165.
- Shephard, N. (1993). Distribution of the ML Estimator of an MA(1) and a Local Level Model. *Econometric Theory*, 9:377–401.
- Stock, J. H. and Watson, M. W. (1996). Evidence on structural instability in macroeconomic time series relation. *Journal of Business and Economic Statistics*, 14(1):11–30.

List of Figure legends

Fig. 1: Estimation of time-varying coefficient model with random-walk dynamics

Fig. 2: Impulse response from a single GtC of emissions

Fig. 3: Estimates of the time-varying parameters and 95% confidence bands, from Extended Kalman Filter and Smoother

Fig. 4: Smoothed states from the EKF estimation of the nonlinear model. Shown are the smoothed processes according to the recursions in Durbin and Koopman (2012, page 237)

Fig. 5: Validation exercise on subsample 2011–2020

Fig. 6: Fitted forecast model for SOI

Fig. 7: Residuals from forecast model for SOI

Fig. 8: Forecasts for SOI